Preparation of sulfide solid electrolytes in the Li_2S-P_2S_5 system by a liquid phase process

Marcela Calpa[a], Nataly Carolina Rosero-Navarro[b*], Akira Miura[b] and Kiyoharu Tadanaga[b]

[a.] Graduate School of Chemical Sciences and Engineering, Hokkaido University, Sapporo 060-8628, Japan

[b.] Division of Applied Chemistry, Faculty of Engineering, Hokkaido University, Sapporo 060-8628, Japan

Corresponding Author

*E-mail address: rosero@eng.hokudai.ac.jp

Abstract

Sulfide solid electrolytes in the Li_2S-P_2S_5 system were synthesized by a liquid phase process under ultrasonic irradiation, and heat treatments at low temperatures. Crystal phase, structure, morphology and ionic conductivity of the sulfide electrolytes were examined after solvent removal at 180 °C and two different heat treatment temperatures, 220 °C and 250 °C. The study revealed that the ionic conductivity of the $xLi_2S\cdot(100-x)P_2S_5$ sulfide electrolytes, in compositions with $70\leq x\leq 75$ mol%, is largely influenced by the local structure. The heat treatment at 220 °C was found to be enough to promote the crystallization of the high ionic conductive $Li_7P_3S_{11}$ phase, higher temperatures for heat treatment as 250 °C leads to the formation of the $P_2S_6^{4-}$ (*hypo*-thiodiphosphate) units in the local structure of the sulfide electrolytes leading to a reduction of the ionic conductivity. The formation and distribution of PS_4^{3-} (*ortho*-thiophosphate), $P_2S_7^{4-}$ (*pyro*-thiophosphate) and $P_2S_6^{4-}$ units in the local structure were found to be key factors to achieve higher ionic conductivity (up to 10^{-3} - 10^{-4} S cm^{-1} at room temperature).

Introduction

All-solid-state lithium batteries with inorganic solid electrolytes have been proposed as the next generation batteries because of the improve safety. Moreover, solid electrolytes with wider electrochemical window enable higher energy density in the all-solid-state battery, because their compatibility with high voltage cathodes[1-3].

Oxide electrolytes such as perovskites[4], NASICON-type[5-8] and garnet-type[9-13] have high ionic conductivities of around 10^{-3} S cm^{-1}, however they require high temperature for the synthesis and subsequent co-sintering to achieve good contact with active materials in the composite cathode of the bulk-type all-solid-state batteries. Sulfide solid electrolytes in the Li_2S-GeS_2-P_2S_5 and Li_2S-P_2S_5 systems, such as $Li_{10}GeP_2S_{12}$[3], $Li_{9.54}Si_{1.74}P_{1.44}S_{11.7}Cl_{0.3}$[14] and $Li_7P_3S_{11}$[15] glass-ceramics, exhibit high ionic conductivity up to 10^{-3} S cm^{-1}. In addition, they also have good ductility that facilitate intimate contact with electrode materials. Therefore, sulfide electrolytes with high ionic conductivity and good mechanical properties would be more suitable solid electrolytes for their application to the all-solid-state battery.

Preparation of sulfide-based solid electrolytes in the Li_2S-P_2S_5 system, often involves preparation of mother glasses by mechanical milling and subsequent

crystallization by heat treatment that leads to an enhancement of the conducting properties. The ionic conductivity of the sulfide glass ceramics highly depends on the precipitation of these crystalline phases. Mizuno et al.[15, 16] found that the crystalline phases are controlled by the x content of Li_2S in the $xLi_2S{\cdot}(100\text{-}x)P_2S_5$ sulfide electrolytes. The precipitation of crystal phases such as $Li_7P_3S_{11}$ by heat treatment at 250-360 °C, in compositions between 70 and 80 mol% Li_2S, produces an enhancement of the conductivity up to 10^{-3} S cm^{-1} at room temperature. Local structure of the glass-ceramics was found to be formed by *pyro*-thiophosphate ($P_2S_7^{4-}$) and *ortho*-thiophosphate (PS_4^{3-}) units. Crystallization of $Li_7P_3S_{11}$ crystal phase is produced at 360°C with a conductivity of 3.2 x 10^{-3} S cm^{-1} at room temperature[15, 17]. In contrast, the precipitation of other crystal phases such as $Li_4P_2S_6$ produces a negative effect on the ionic conductivity, a decreasing of down to two orders of magnitude have been reported (1.1 x 10^{-6} S cm^{-1} at room temperature).[17]

Recently, the synthesis of sulfide solid electrolytes by liquid phase has been reported as an alternative method to the mechanical milling. It was found that the reaction between Li_2S and P_2S_5 can be mediated by organic solvents under magnetic stirring. This chemical synthesis is a very low energy process in comparison to the mechanical milling process. Crystalline phases such as

Li_3PS_4 and $Li_7P_3S_{11}$ has been obtained by a liquid phase synthesis using different solvents such as 1,2-dimethoxyethane[18], ethyl acetate[19], n-methylformamide[20], tetrahydrofuran[21] or acetonitrile[22] as mediators. We found[23] that $Li_7P_3S_{11}$ with high ionic conductivity up to 1 $x10^{-3}$ S cm^{-1} at room temperature and low activation energy of 12.8 KJ mol^{-1}, can be synthesized from Li_2S and P_2S_5 by an instantaneous procedure involving a liquid phase process and low heat treatment at 220 °C. The ionic conductivity was to be largely related to the local structure. Structure rearrangement promoted by heat treatment led to an increase of $P_2S_7^{4-}$ units in the structure of the sulfide electrolyte involving an increase in the ionic conductivity[23].

Motivated by these findings[23], in this work, the influence of heat treatment and composition in the Li_2S-P_2S_5 system on the structure and properties of the sulfide electrolytes synthesized by an instantaneous liquid phase process[23] were investigated. To examine the effect of heat treatment, $xLi_2S\cdot(100-x)P_2S_5$ sulfide electrolytes with 70 and 75 mol% Li_2S content, were studied after solvent removal (180 °C) and heat treatment at 220 °C and 250 °C, using X-ray diffraction (XRD), Raman spectroscopy, scanning electron microscopy (SEM) and electrochemical impedance (EIS). The results revealed that sulfide solid electrolytes with high ionic conductivity can be obtained at the heat treatment temperature of 220°C. To

investigate the influence of the composition, $xLi_2S·(100-x)P_2S_5$ sulfide electrolytes in compositions with 70≤x≤75 mol%, were studied after heat treatment at 220 °C, using similar techniques.

Experimental section

Synthesis

Li_2S (Mitsuwa Chemical, 99.9%) and P_2S_5 (Aldrich, 99%) in the stoichiometry compositions (70:30, 71:29, 72:28, 73:27, 74:26 and 75:25 mol%) were mixed in anhydrous acetonitrile (Wako Pure Chemical Industries). Each mixture was ultrasonicated at 60°C for 30 min under 28 kHz using an ultrasonic bath (Shimadzu SUS-103). The ultrasonication process formed a white suspension in all samples. The suspension was dried at 180 °C for 3 h under vacuum to remove the solvent and obtain solid powders. Subsequently, the powders were heat treated at 220°C or 250°C for 1 h to promote the crystallization. The samples were named using the composition followed by the specific condition. For example, $70Li_2S·30P_2S_5$-180 correspond to the sample prepared from Li_2S and P_2S_5 in the composition 70:30 mol%, after the drying process at 180°C.

Structural and electrochemical characterization

Crystal phase and chemical composition of the sulfide electrolytes were studied by X-ray diffraction (XRD) and Raman spectroscopy. XRD measurements were

performed using a CuKα radiation with an X-ray diffractometer (Miniflex 600, Rigaku). Diffraction data were collected in 0.01° steps from 10° to 40° in 2θ. The XRD patterns were indexed using the Rigaku PDXL Software. Raman spectroscopy was performed using a Raman spectrometer (HORIBA XploRA PLUS Scientific). Raman spectra were recorded between 300 and 500 cm^{-1}. Morphology of the sulfide solid electrolyte particles was observed by scanning electron microscopy (SEM), performed on a JIB-4600F Multibeam SEM-FIB Scanning Electron Microscope.

The ionic conductivity of the pelletized samples was evaluated by electrochemical impedance spectroscopy (EIS). The solid electrolyte powders (80 mg) were pressed under 360 MPa (at room temperature) in a polycarbonate tube, with 10 mm of diameter, two stainless steel (SS) disks were used as current collectors. EIS was measured using an impedance analyser (SI 1260, Solartron) in the frequency range from 0.1 Hz to 1 MHz at the amplitude of 30 mV. The spectra were analyzed with the ZView software (Version 3.3f, Scribner Associates) in order to assess the ohmic resistance (R) of the pellet. All processes were performed in an Argon atmosphere.

Results and discussion

To study the effect of heat treatment on the structure and properties of the sulfide

electrolytes synthesized by an instantaneous liquid phase process, $xLi_2S\cdot(100-x)P_2S_5$ sulfide electrolytes with 70 and 75 mol% Li_2S content were selected. The solid electrolytes were studied after solvent removal (180 °C) and after heat treatment (220 °C and 250 °C), by using X-ray diffraction, Raman spectroscopy, scanning electron microscopy and electrochemical impedance.

Figure 1a shows the XRD pattern of the sulfide solid electrolyte $70Li_2S\cdot30P_2S_5$, after solvent removal at 180°C, and heat treatment at 220°C and 250°C. Indexed XRD pattern of the $Li_7P_3S_{11}$ (ICDD#157654), $Li_4P_2S_6$ (ICDD#80319) and γ-Li_3PS_4 (ICD#180318) phases are shown for comparison. The XRD pattern of the $70Li_2S\cdot30P_2S_5$-180 sample shows a complex pattern with unknown peaks. A peak corresponding to Li_2S was identified, but the other peaks were not able to be associated to P_2S_5 precursor or any solid electrolyte phases. The XRD pattern was indexed by a tetragonal cell with space group p4/m(83) and lattice parameters of a=b=8.5930 and c=12.7620. It is considered a single phase because all peaks could be indexed (details are given at Figure S1 and Table S1 of the supporting information). The XRD pattern of the $70Li_2S\cdot30P_2S_5$-220 sample shows the presence of the $Li_7P_3S_{11}$, $Li_4P_2S_6$ and γ-Li_3PS_4 phases. The presence of unknown peaks was also observed. These peaks do not match with the peaks observed in the $70Li_2S\cdot30P_2S_5$-180 sample. Thus, secondary phases

may have been formed. The XRD pattern of the $70Li_2S{\cdot}30P_2S_5$-250 sample shows the formation of $Li_4P_2S_6$ as main phase.

Figure 1b shows the Raman spectra of the sulfide solid electrolyte $70Li_2S{\cdot}30P_2S_5$, corresponding to the same conditions of the XRD study (figure 1a). Raman spectrum of the $70Li_2S{\cdot}30P_2S_5$-180 sample shows two main bands, at 428 cm^{-1} and 391 cm^{-1}, attributed to the PS_4^{3-} and $P_2S_6^{4-}$ units[24], which confirms the formation of the P_xS_y units by the liquid phase synthesis. The Raman spectrum of the $70Li_2S{\cdot}30P_2S_5$-220 sample shows the two bands located at 380 cm^{-1} and 405 cm^{-1} and the appearance of a new band at 428 cm^{-1} attributed to $P_2S_7^{4-}$ units[24]. The Raman spectrum of the $70Li_2S{\cdot}30P_2S_5$-250 sample shows only a main band at 380 cm^{-1}($P_2S_6^{4-}$).

Figure 2a shows the XRD Pattern of the sulfide solid electrolyte $75Li_2S{\cdot}25P_2S_5$, after solvent removal at 180°C, and heat treatment at 220°C and 250°C. Indexed XRD pattern of the $Li_7P_3S_{11}$ (ICDD#157654), $Li_4P_2S_6$ (ICDD#80319) and υ-Li_3PS_4 (ICD#180318) phases are shown for comparison. The XRD pattern of the $75Li_2S{\cdot}25P_2S_5$-180 sample shows a complex pattern with unknown peaks located at the same 2θ positions of the sample $70Li_2S{\cdot}30P_2S_5$-180. The XRD pattern was indexed by a tetragonal cell with space group p4/m(83) and lattice parameters of a=b=19.2157 and c=6.3772 (details are given at Figure S2 and

Table S2 of the supporting information). The XRD pattern of the $75Li_2S{\cdot}25P_2S_5$-220 sample shows the presence of $Li_7P_3S_{11}$ as main phase. The presence of Li_2S phase was also identified. The $75Li_2S{\cdot}25P_2S_5$-250 sample shows a similar XRD pattern to the $75Li_2S{\cdot}25P_2S_5$-220 sample.

Figure 2b shows the Raman spectra of the sulfide solid electrolyte $75Li_2S{\cdot}25P_2S_5$, corresponding to the same conditions of the XRD study (figure 2a). Raman spectrum of the $75Li_2S{\cdot}25P_2S_5$-180 sample shows a wide band at 428 cm^{-1} denoting the formation of the PS_4^{3-} units. The Raman spectrum of the $75Li_2S{\cdot}25P_2S_5$-220 sample shows a band located at 428 cm^{-1} and the appearance of a new band located at 405 cm^{-1} corresponding to $P_2S_7^{4-}$ units. Raman spectrum of the $75Li_2S{\cdot}25P_2S_5$-250 sample shows only a wide band centered at 405 cm^{-1}. Figure 2c corresponds to the deconvolution of the Raman spectrum of the $75Li_2S{\cdot}25P_2S_5$-250 sample, using a Gaussian-Lorentzian function. Deconvolution shows that the wide band was composed by three bands centered at 420 cm^{-1}, 404 cm^{-1} and 385 cm^{-1}, corresponding to the PS_4^{3-} and $P_2S_7^{4-}$ units and the new formation of $P_2S_6^{4-}$ units in the $75Li_2S{\cdot}25P_2S_5$-250 sample.

Figure 3 displays the morphology of the $70Li_2S{\cdot}30P_2S_5$ and $75Li_2S{\cdot}25P_2S_5$ samples, after solvent removal at 180°C, and heat treatment at 220°C and 250°C.

Figure 3a-c display SEM micrographs of the $70Li_2S{\cdot}30P_2S_5$-180, $70Li_2S{\cdot}30P_2S_5$-220 and $70Li_2S{\cdot}30P_2S_5$-250 samples, correspondingly. Big agglomerates, with a size range between 5 μm and 20 μm, were observed in the $70Li_2S{\cdot}30P_2S_5$-180 sample. The $70Li_2S{\cdot}30P_2S_5$-220 and $70Li_2S{\cdot}30P_2S_5$-250 samples consisted of small particles with particle size bellow 500 nm, however, agglomeration was also observed. Figure 3d-f display SEM micrographs of the $75Li_2S{\cdot}25P_2S_5$-180, $75Li_2S{\cdot}25P_2S_5$-220 and $75Li_2S{\cdot}25P_2S_5$-250 samples, correspondingly. The $75Li_2S{\cdot}25P_2S_5$-180 sample shows big agglomerates as the $70Li_2S{\cdot}30P_2S_5$-180 sample. The $75Li_2S{\cdot}25P_2S_5$-220 and $75Li_2S{\cdot}25P_2S_5$-250 samples show irregular particle size of around 500 nm, slightly larger than the particle size of the $70Li_2S{\cdot}30P_2S_5$-220 and $70Li_2S{\cdot}30P_2S_5$-250 samples.

The ionic conductivity of the $70Li_2S{\cdot}30P_2S_5$ and $75Li_2S{\cdot}25P_2S_5$ samples was evaluated by electrochemical impedance spectroscopy (EIS). Figure 4a shows the impedance spectra of the $70Li_2S{\cdot}30P_2S_5$-220 and $70Li_2S{\cdot}30P_2S_5$-250 pelletized samples. The impedance spectra of both samples consist of a semicircle at high frequency and a capacitive tail at low frequency due to the electrodes interface. For each sample, the data was fitted with a simple equivalent circuit comprising a resistor in parallel with a capacitor *(R||C, C is a constant phase element)* to describe the pellet electrical behavior. In addition, a

capacitor in series was used to simulate the contribution of the electrodes interface. The fitting results were drawn together with each EIS data. The total resistance (bulk and grain boundary resistances), was used to calculate the ionic conductivity. The $70Li_2S{\cdot}30P_2S_5$-220 and $70Li_2S{\cdot}30P_2S_5$-250 samples attained 1.1 x 10^{-5} Scm^{-1} and 3.7 x 10^{-6} Scm^{-1}, correspondingly. Figure 4b shows the impedance spectra of the $75Li_2S{\cdot}25P_2S_5$-220 and $75Li_2S{\cdot}25P_2S_5$-250 pelletized samples. The impedance spectra of both samples do not exhibit the full semicircle due to the lower resistance. The resistance was estimated by the value of Z' at the intercept with the real axis obtained by linear fitting. The ionic conductivity of the $75Li_2S{\cdot}25P_2S_5$-220 and $75Li_2S{\cdot}25P_2S_5$-250 samples attained 6.4 x 10^{-4} Scm^{-1} and 6.1 x 10^{-4} Scm^{-1}, correspondingly.

The evaluation of the $70Li_2S{\cdot}30P_2S_5$ and $75Li_2S{\cdot}25P_2S_5$ samples by XRD diffraction and Raman spectroscopy revealed a different local structure depending on their composition and heat treatment. At 180 °C, similar XRD patterns were observed in both solid electrolytes, exposing a similar reaction state. However, the Raman spectra displays clearly that the solid electrolytes contain different structural units. The formation of PS_4^{3-} units was observed in both compositions, but $P_2S_6^{4-}$ units was only observed at lower Li_2S content. As reported in a previous study[23], acetonitrile is completely removed at 220°C,

however at 180 °C Raman bands corresponding to acetonitrile are still observed. Although there is no evidence at this moment, the remained acetonitrile in the samples at 180 °C, suggest that the undefined crystal phase correspond to the formation of complex between the solvent and the P_xS_y units[23]. Indexing of the XRD patterns reveals the formation of a single phase with space group p4/m(83) in both compositions, however different lattice parameters were calculated for each composition. The different arrangement of the P_xS_y units may influence the interaction between the solvent and the sulfide electrolytes, resulting in the different lattice parameters. Heat treatment at 220°C completely removed the solvent and promoted the formation of $P_2S_7^{4-}$ units in both samples. Higher temperature of 250°C led to the formation of $Li_4P_2S_6$ and $Li_7P_3S_{11}$ crystal phases in the $70Li_2S{\cdot}30P_2S_5$-250 and $75Li_2S{\cdot}25P_2S_5$-250 samples, respectively. The presence of the $P_2S_6^{4-}$ units was also confirmed in the $75Li_2S{\cdot}25P_2S_5$-250 sample by the deconvolution of the observed band (figure 2c). Higher formation of $P_2S_6^{4-}$ units at higher temperature for the heat treatment has also been observed in the sulfide solid electrolytes synthesized by mechanical milling[25]. Both compositions presented a small particle size around 500 nm after heat treatments. The different compositions or the different temperatures at heat treatment do not significantly affect the morphology. The smaller particle obtained

by liquid phase has been previously reported [22, 26]. The particle size is more than 10 times smaller compared with the particle size obtained by mechanical milling process (10 μm)[27]. The small particle size is attributed to the interaction between solvent and particles during the synthesis process. The acetonitrile can remain on the surface of individual particles, leading to obtain a better dispersion of the powder during the ultrasonication and further a good control of the particle size growth during the solvent removal[28].

The ionic conductivity of the $75Li_2S{\cdot}25P_2S_5$-220 sample was more than one order of magnitude higher than the $70Li_2S{\cdot}30P_2S_5$-220 sample. Although, XRD patterns of both sulfide electrolytes showed the formation of the high conductive $Li_7P_3S_{11}$ crystal phase, the presence of $P_2S_6^{4-}$ units in the local structure of the $70Li_2S{\cdot}30P_2S_5$-220 sample is considered as the main reason of lower ionic conductivity. Regarding the heat treatment at 250 °C, the ionic conductivity of the $70Li_2S{\cdot}30P_2S_5$-250 sample was around one order of magnitude lower in comparison with the $70Li_2S{\cdot}30P_2S_5$-220 sample. The reduction of the ionic conductivity is expected since the higher heat treatment promoted the crystallization of the lower ionic conductor $Li_4P_2S_6$ phase, as confirmed by XRD and Raman spectroscopy. On the other hand, the heat treatment at 250 °C of the $75Li_2S{\cdot}25P_2S_5$ sample did not produce a significative change in terms of ionic

conductivity in comparison with the sample heated at 220 °C. The $Li_7P_3S_{11}$ crystal phase (figure 2a) was confirmed at 220 °C and 250 °C, but the existence of $P_2S_6^{4-}$ units (figure 2c) in the $75Li_2S{\cdot}25P_2S_5$-250 sample was associated to the slight loss of ionic conductivity.

The heat treatment at 220 °C was enough to promote the formation of the $P_2S_7^{4-}$ units, higher temperatures for heat treatment as 250 °C leads to the formation of the $P_2S_6^{4-}$ units involving a reduction of the ionic conductivity. Therefore, to study the effect of composition in the Li_2S-P_2S_5 system on the structure and properties of the sulfide electrolytes synthesized by an instantaneous liquid phase process[23], the temperature of 220 °C was chosen for the heat treatment.

To investigate the influence of composition, the structure and ionic conductivity of $xLi_2S{\cdot}(100\text{-}x)P_2S_5$ sulfide solid electrolytes, with 70, 71, 72, 73, 74 and 75 mol% Li_2S content, after heat treatment at 220 °C, were studied by using X-ray diffraction, Raman spectroscopy, and electrochemical impedance.

Figure 5a shows the XRD pattern of the $xLi_2S{\cdot}(100\text{-}x)P_2S_5$ sulfide electrolytes after heating at 220 °C. The $Li_7P_3S_{11}$ crystalline phase was observed in the XRD patterns of all the studied compositions. Formation of $Li_4P_2S_6$ and γ-Li_3PS_4 phases were only observed in the $70Li_2S{\cdot}30P_2S_5$-220 and $71Li_2S{\cdot}29P_2S_5$-220 compositions with the presence of some peaks with unknown structure.

Figure 5b shows the Raman spectra of the $xLi_2S·(100-x)P_2S_5$ sulfide electrolytes after heating at 220 °C. The Raman spectrum of the $75Li_2S·25P_2S_5$-220 sample shows two bands located at 428 cm^{-1} and 405 cm^{-1} corresponding to of PS_4^{3-} and $P_2S_7^{4-}$ units. The Raman spectrum of the $74Li_2S·26P_2S_5$-220 sample shows a wide band located at 405 cm^{-1} corresponding mainly to $P_2S_7^{4-}$ units, and PS_4^{3-} and $P_2S_6^{4-}$ units in less proportion. The Raman spectrum of the $73Li_2S·27P_2S_5$-220 sample shows two wide bands centered at 405 cm^{-1} and 385 cm^{-1}, corresponding mainly to $P_2S_7^{4-}$ and $P_2S_6^{4-}$ units, and PS_4^{3-} units in less proportion. The Raman spectrum of the $72Li_2S·28P_2S_5$-220 sample shows two wide bands centered at 405 cm^{-1} and 385 cm^{-1}, corresponding to $P_2S_7^{4-}$ and $P_2S_6^{4-}$ units. The Raman spectrum of the $71Li_2S·29P_2S_5$-220 sample shows similar bands to the $72Li_2S·28P_2S_5$-220 sample, with a slightly increase of the band at 405 cm^{-1}. The Raman spectrum of the $70Li_2S·30P_2S_5$-220 sample shows three bands located at 428 cm^{-1}, 405 cm^{-1} and 385 cm^{-1} corresponding to $P_2S_6^{4-}$ units, $P_2S_7^{4-}$ and PS_4^{3-} units.

Figure 6 shows the ionic conductivity of the $xLi_2S·(100-x)P_2S_5$ sulfide electrolytes after heating at 220 °C. The attained ionic conductivity of the $xLi_2S·(100-x)P_2S_5$ sulfide electrolytes with 70, 71, 72, 73, 74 and 75 mol% Li_2S content, was 1.1 x 10^{-5} S cm^{-1}, 3.4 x 10^{-5} S cm^{-1}, 5.8 x 10^{-5} S cm^{-1}, 1.5 x 10^{-4} S cm^{-1}, 1.0 x 10^{-3} S cm^{-1} and 6.4 x 10^{-4}

S cm^{-1}, respectively. The ionic conductivity increases with the Li_2S content until a maximum value of 10^{-3} S cm^{-1} with 74 mol% Li_2S. The difference of ionic conductivity between the $xLi_2S·(100-x)P_2S_5$ compositions achieved up to two orders of magnitude.

The study of the $xLi_2S·(100-x)P_2S_5$ sulfide electrolytes after heating at 220 °C suggests that the variation of ionic conductivity is largely influenced by the resulting crystalline phases and the local arrangement of the P_xS_y units. Although the $Li_7P_3S_{11}$ high ionic conductor was identified in all the compositions (XRD spectroscopy, Figure 5a), the distribution of P_xS_y units was clearly different for each composition (Raman spectroscopy, Figure 5b). Lower ionic conductivity (~10^{-5} S cm^{-1}) resulted from $xLi_2S·(100-x)P_2S_5$ sulfide electrolytes with low content of Li_2S (x = 70-71); attributed to the presence of the low ionic conductive phases, $Li_4P_2S_6$ and ϒ-Li_3PS_4[29], confirmed by XRD spectroscopy (Figure 5a). Further, the slightly increase of the Li_2S content (x = 72-73) was enough to remove the presence of the low ionic conductive phases, producing an improvement of the ionic conductivity up to one order of magnitude (~10^{-4} S cm^{-1}). The significantly higher presence of $P_2S_6^{4-}$ units in comparison with PS_4^{3-} and $P_2S_7^{4-}$ units (observed by Raman spectroscopy, Figure 5b) was assumed as main reason for the relatively low ionic conductivity. Higher content of Li_2S (x = 74-75)

produced the highest ionic conductivity (~10^{-3} – 10^{-4} S cm^{-1}) in the $xLi_2S\cdot(100-x)P_2S_5$ solid electrolytes obtained by the liquid phase process. Since the XRD patterns do not exhibited considerable changes in the $Li_7P_3S_{11}$ phase, for example compared to the composition with 72 - 73 mol% Li_2S, the high ionic conductivity can be interpreted by the optimized arrangement of the P_xS_y units. Raman spectrum of the sulfide electrolyte with 74 mol% Li_2S, with the highest ionic conductivity of 10^{-3} S cm^{-1}, revealed that the presence of the $P_2S_7^{4-}$ units (respect to PS_4^{3-} and $P_2S_6^{4-}$ units), is significantly higher compared to the sulfide electrolyte with 75 mol% Li_2S. It can be inferred that high content of $P_2S_7^{4-}$ units in the structure of the $xLi_2S\cdot(100-x)P_2S_5$ sulfide electrolytes resulted in the formation of high ionic conductive materials. The ionic conductivity of the $xLi_2S\cdot(100-x)P_2S_5$ solid electrolytes synthesized by liquid phase show a similar tendency of the $xLi_2S\cdot(100-x)P_2S_5$ glasses obtained by mechanical milling process *(*as high Li_2S content as high ionic conductivity[15]*)*, however, the crystallization behavior is quite different.[15, 30] By the mechanical milling process, the superionic crystalline phases with ionic conductivity around 10^{-3} S cm^{-1} are obtained by a careful heat treatment of the $xLi_2S\cdot(100-x)P_2S_5$ glasses. The $75Li_2S\cdot25P_2S_5$ glass obtained by mechanical milling contains PS_4^{3-} units as main structural unit (PS_4^{3-} and $P_2S_7^{4-}$ units in lower proportion)[30] and the Li_3PS_4 crystal phase has been confirmed after the first crystallization temperature at 220 –

260 °C.[15] The $75Li_2S{\cdot}25P_2S_5$ solid electrolyte obtained by liquid phase only showed the formation of PS_4^{3-} units as main structural unit after the solvent removal at 180 °C (figure 2b) and the further heat treatment at 220 °C led to the crystallization of the $Li_7P_3S_{11}$ phase and the formation of the $P_2S_7^{4-}$ units (figure 5a-b).

Although the exact reason of the crystallization behavior of the $xLi_2S{\cdot}(100\text{-}x)P_2S_5$ solid electrolytes synthesized by liquid phase is still unknown, the local structures obtained by the ultrasonication process are considered as the main reason of this difference with the mechanical milling process. The ultrasonication process produce not only the particle disaggregation (confirmed by SEM, Figure 3), but also an enhancement of the chemical reactivity. The local high temperatures and pressures generated by the further cavitation, leads to a chemical state very different to that obtained after the mechanical milling process.

The optimization of the heat treatment temperature and the Li_2S content are necessary for obtaining high ionic conductivity in the $xLi_2S{\cdot}(100\text{-}x)P_2S_5$ solid electrolytes synthesized by an instantaneous liquid phase process. Further studies, by using techniques such as synchrotron X-ray diffraction, will be done to elucidate the crystallization behavior of the sulfide electrolytes.

Conclusions

In summary, structure and properties of $xLi_2S·(100-x)P_2S_5$ solid electrolytes, in compositions with 70≤x≤75 mol%, synthesized by an instantaneous liquid phase process and subsequent heat treatment have been examined by using X-ray diffraction, Raman spectroscopy, scanning electron microscopy and electrochemical impedance.

It was found that heat treatment at 220 °C is enough to promote the formation of the $P_2S_7^{4-}$ units, favoring a high ionic conductivity. The heat treatment at 250 °C leads to the formation of the $P_2S_6^{4-}$ units leading a reduction of the ionic conductivity. A small particle size of around 500 nm was observed in the sulfide electrolytes. The heat treatment temperatures do not significantly affect the morphology.

As was expected, the Li_2S content played an important role in the structure and electrochemical properties of the $xLi_2S·(100-x)P_2S_5$ solid electrolytes. The $Li_7P_3S_{11}$ crystalline phase was observed in the XRD patterns of all the studied compositions after the heat treatment at 220 °C. However, it was found that the Li_2S content largely influence the distribution of the P_xS_y units in the local structure of the sulfide electrolytes. A higher content of $P_2S_7^{4-}$ unit was determinant to obtain the highest ionic conductivity. The high ionic conductivity of 1

x 10^{-3} S cm^{-1} at 22 °C was obtained in the solid electrolyte with Li_2S content of 74 mol% after the heat treatment at 220 °C.

Acknowledgments

The present work was supported by the Japan Science and Technology Agency (JST), Advanced Low Carbon Technology Research and Development Program (ALCA), and Specially Promoted Research for Innovative Next Generation Batteries (SPRING) project. The analysis of SEM was carried out with JIB-4600F at the “Joint-use Facilities: Laboratory of Nano-Micro Material Analysis”, Hokkaido University, supported by “Material Analysis and Structure Analysis Open Unit (MASAOU)”.

References

1. J. C. Li, C. Ma, M. F. Chi, C. D. Liang and N. J. Dudney, *Adv. Energy Mater*, 2015, **5**, 1-6.
2. Z. C. Liu, W. J. Fu, E. A. Payzant, X. Yu, Z. L. Wu, N. J. Dudney, J. Kiggans, K. L. Hong, A. J. Rondinone and C. D. Liang, *J. Am. Chem. Soc.*, 2013, **135**, 975-978.
3. N. Kamaya, K. Homma, Y. Yamakawa, M. Hirayama, R. Kanno, M. Yonemura, T. Kamiyama, Y. Kato, S. Hama, K. Kawamoto and A. Mitsui, *Nat. Mater.*, 2011, **10**, 682-686.
4. M. Itoh, Y. Inaguma, W. H. Jung, L. Q. Chen and T. Nakamura, *Solid State Ionics*, 1994, **70**, 203-207.
5. C. R. Mariappan, C. Yada, F. Rosciano and B. Roling, *J. Power Sources*, 2011, **196**, 6456-6464.
6. M. Gellert, K. I. Gries, C. Yada, F. Rosciano, K. Volz and B. Roling, *J. Phys. Chem. C*, 2012, **116**, 22675-22678.
7. J. S. Thokchom, N. Gupta and B. Kumar, *J. Electrochem. Soc.*, 2008, **155**, A915-A920.
8. P. Hartmann, T. Leichtweiss, M. R. Busche, M. Schneider, M. Reich, J. Sann, P.

Adelhelm and J. Janek, *J. Phys. Chem. C*, 2013, **117**, 21064-21074.

9. V. Thangadurai, H. Kaack and W. J. F. Weppner, *J. Am. Ceram. Soc.*, 2003, **86**, 437-440.

10. V. Thangadurai and W. Weppner, *Adv. Funct. Mater.*, 2005, **15**, 107-112.

11. R. Murugan, V. Thangadurai and W. Weppner, *Angew. Chem. Int. Ed.*, 2007, **46**, 7778-7781.

12. H. Buschmann, J. Dolle, S. Berendts, A. Kuhn, P. Bottke, M. Wilkening, P. Heitjans, A. Senyshyn, H. Ehrenberg, A. Lotnyk, V. Duppel, L. Kienle and J. Janek, *Phys. Chem. Chem. Phys*, 2011, **13**, 19378-19392.

13. N. C. Rosero-Navarro, T. Yamashita, A. Miura, M. Higuchi and K. Tadanaga, *J. Am. Ceram. Soc.*, 2017, **100**, 276-285.

14. Y. Kato, S. Hori, T. Saito, K. Suzuki, M. Hirayama, A. Mitsui, M. Yonemura, H. Iba and R. Kanno, *Nat. Energy*, 2016, **1**, 16030.

15. F. Mizuno, A. Hayashi, K. Tadanaga and M. Tatsumisago, *Solid State Ionics*, 2006, **177**, 2721-2725.

16. F. Mizuno, A. Hayashi, K. Tadanaga and M. Tatsumisago, *Adv. Mater.*, 2005, **17**, 918-921.

17. A. Hayashi, K. Minami and M. Tatsumisago, *J. Solid State Electrochem.*, 2010, **14**, 1761-1767.

18. S. Ito, M. Nakakita, Y. Aihara, T. Uehara and N. Machida, *J. Power Sources*, 2014, **271**, 342-345.

19. N. H. H. Phuc, M. Totani, K. Morikawa, H. Muto and A. Matsuda, *Solid State Ionics*, 2016, **288**, 240-243.

20. S. Teragawa, K. Aso, K. Tadanaga, A. Hayashi and M. Tatsumisago, *J. Mater. Chem. A*, 2014, **2**, 5095-5099.

21. H. Wang, Z. D. Hood, Y. N. Xia and C. D. Liang, *J. Mater. Chem. A*, 2016, **4**, 8091-8096.

22. X. Y. Yao, D. Liu, C. S. Wang, P. Long, G. Peng, Y. S. Hu, H. Li, L. Q. Chen and X. X. Xu, *Nano Lett.*, 2016, **16**, 7148-7154.

23. M. Calpa, N. C. Rosero-Navarro, A. Miura and K. Tadanaga, *RSC Adv.*, 2017, **7**, 46499-46504.

24. M. Tachez, J.-P. Malugani, R. Mercier and G. Robert, *Solid State Ionics*, 1984, **14**, 181-185.

25. M. R. Busche, D. A. Weber, Y. Schneider, C. Dietrich, S. Wenzel, T. Leichtweiss, D. Schroder, W. B. Zhang, H. Weigand, D. Walter, S. J. Sedlmaier, D. Houtarde, L. F. Nazar and J. Janek, *Chem. Mater.*, 2016, **28**, 6152-6165.

26. N. H. H. Phuc, K. Morikawa, M. Totani, H. Muto and A. Matsuda, *Solid State Ionics*, 2016, **285**, 2-5.

27. A. Sakuda, T. Takeuchi and H. Kobayashi, *Solid State Ionics*, 2016, **285**, 112-117.

28. H. Wang, Z. D. Hood, Y. N. Xia and C. D. Liang, *J. Mater. Chem. A*, 2016, **4**, 8091-8096.

29. K. Homma, M. Yonemura, T. Kobayashi, M. Nagao, M. Hirayama and R. Kanno, *Solid State Ionics*, 2011, **182**, 53-58.

30. C. Dietrich, D. A. Weber, S. J. Sedlmaier, S. Indris, S. P. Culver, D. Walter, J. Janek and W. G. Zeier, *J. Mater. Chem. A*, 2017, **5**, 18111-18119.

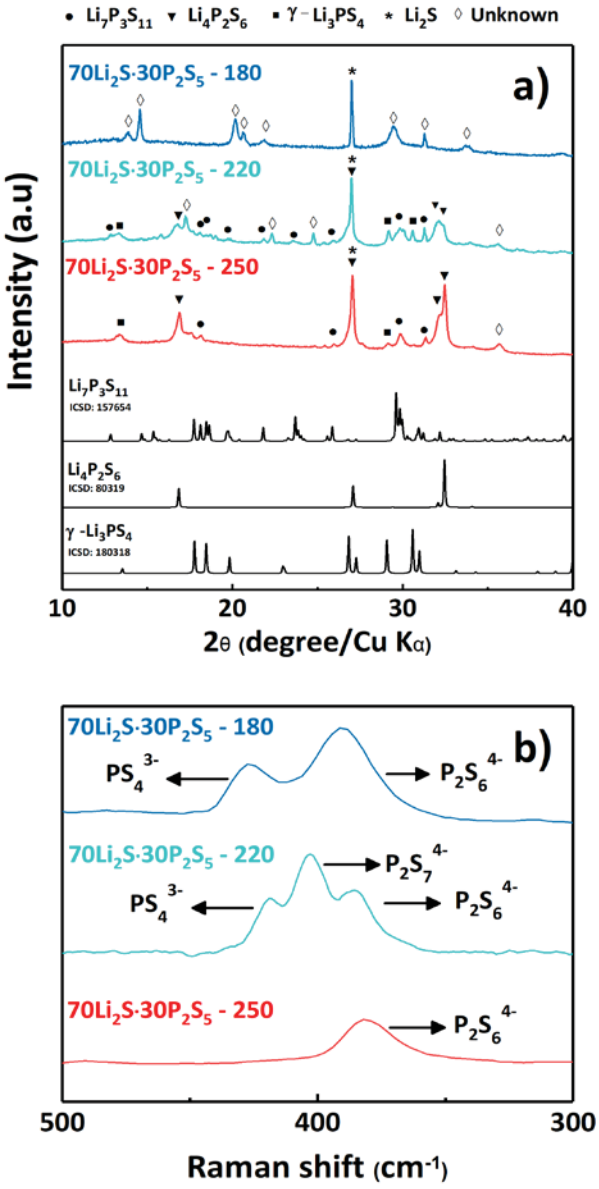

Figure 1. a) XRD Pattern and **b)** Raman spectra of the sulfide solid electrolyte $70Li_2S{\cdot}30P_2S_5$ after solvent removal at 180°C, and heat treatment at 220°C and 250°C.

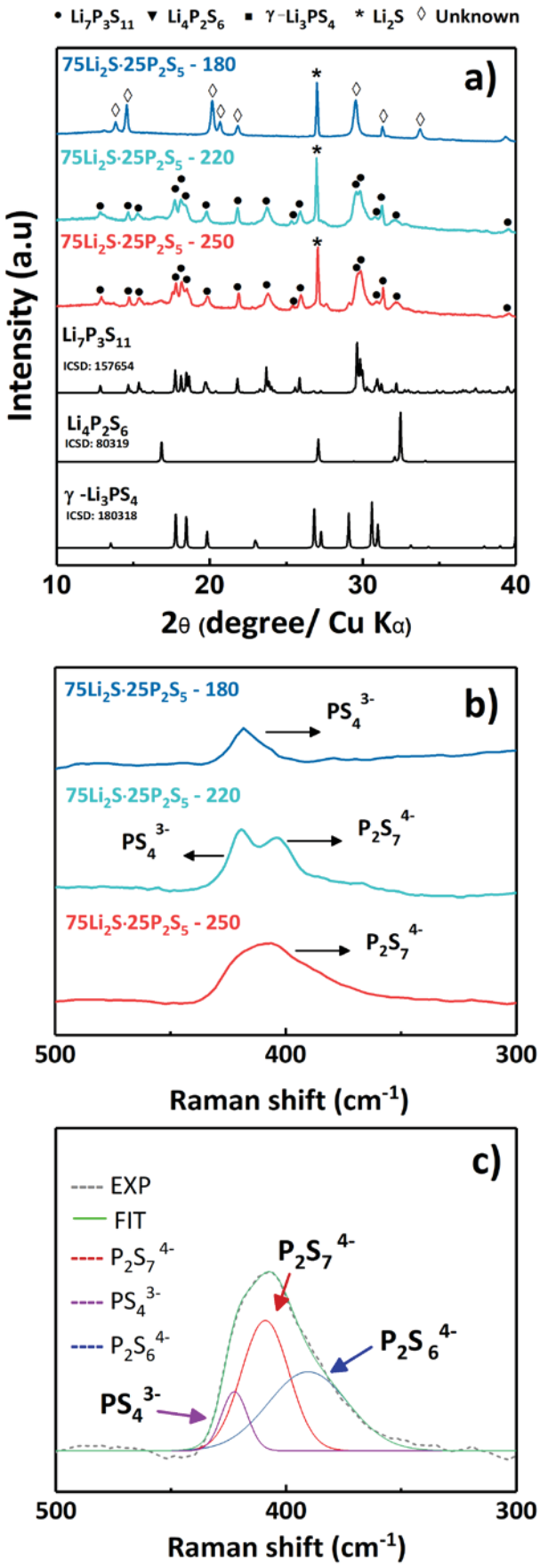

Figure 2. a) XRD Pattern and **b)** Raman spectra of the sulfide solid electrolyte $75Li_2S{\cdot}25P_2S_5$ after solvent removal at 180°C, and heat treatment at 220°C and 250°C. **c)** Spectral decomposition of Raman spectrum for the $75Li_2S{\cdot}25P_2S_5$ - 250 sample. Dashed grey line, experimental data; continuous green line, the fitting result of all P_xS_y polyhedral; Dashed purple, red and blue lines, PS_4^{3-}, $P_2S_7^{4-}$ and $P_2S_6^{4-}$ units, correspondingly.

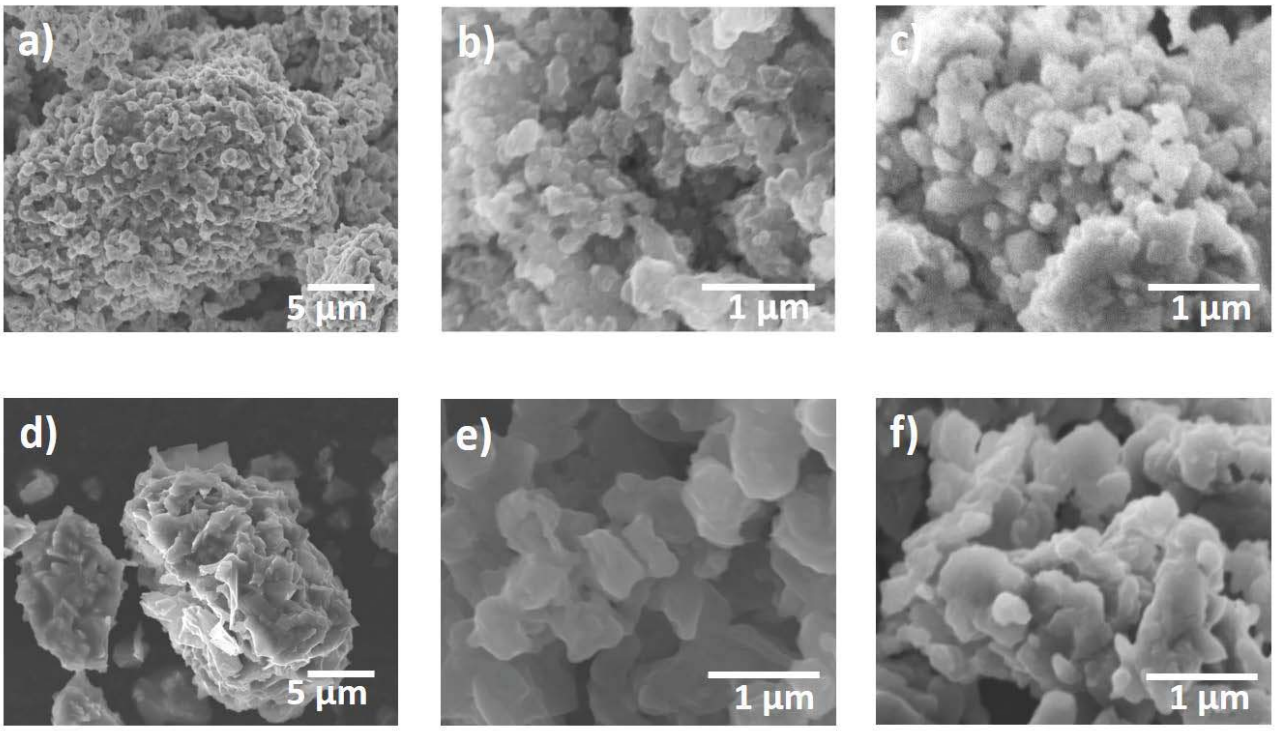

Figure 3. SEM Micrographs of the sulfide electrolytes: **a)** $70Li_2S{\cdot}30P_2S_5$-180, **b)** $70Li_2S{\cdot}30P_2S_5$-220, **c)** $70Li_2S{\cdot}30P_2S_5$-250, **d)** $75Li_2S{\cdot}25P_2S_5$-180, **e)** $75Li_2S{\cdot}25P_2S_5$-220 and **f)** $75Li_2S{\cdot}25P_2S_5$ -250.

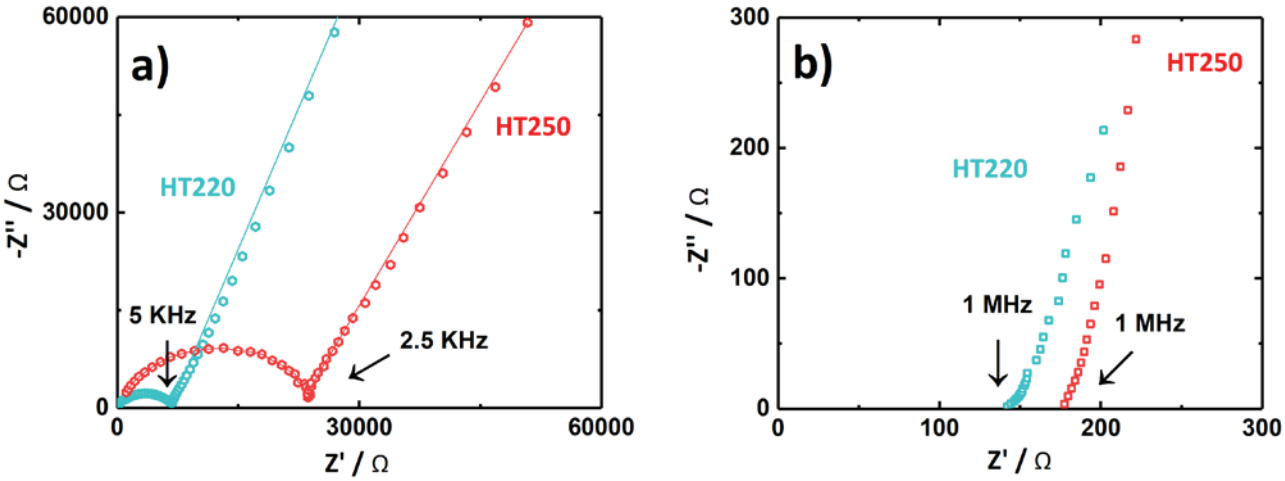

Figure 4. Impedance spectra measured at 22 ˚C of the pelletized samples: **a)** $70Li_2S{\cdot}30P_2S_5$-220 (HT220) and $70Li_2S{\cdot}30P_2S_5$-250 (HT250) and **b)** $75Li_2S{\cdot}25P_2S_5$-220 (HT220) and $75Li_2S{\cdot}25P_2S_5$-250 (HT250).

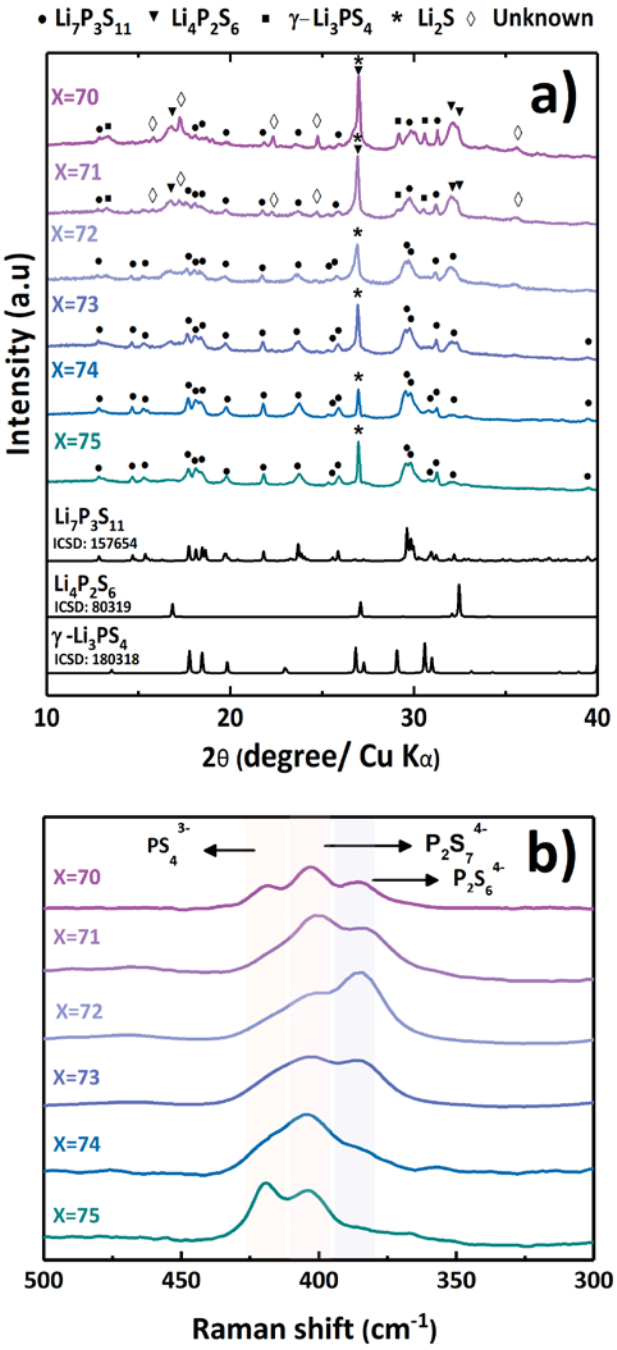

Figure 5. a) XRD Patterns and **b)** Raman spectra of the sulfide solid electrolytes in the $xLi_2S{\cdot}100\text{-}xP_2S_5$ system, obtained by liquid phase and heat treatment at 220 ˚C.

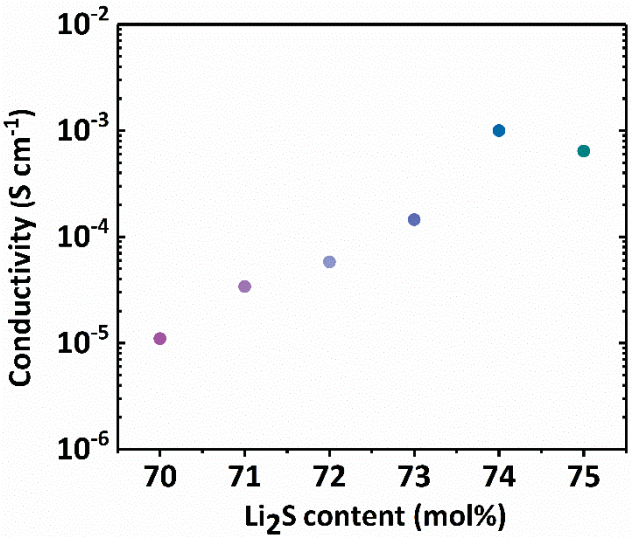

Figure 6 Ionic conductivity of the sulfide solid electrolytes in the $xLi_2S{\cdot}100\text{-}xP_2S_5$ system, obtained by liquid phase and heat treatment at 220 ˚C.

Supplementary Information

Preparation of sulfide solid electrolytes in the Li_2S-P_2S_5 system by a liquid phase process

Marcela Calpa[a], Nataly Carolina Rosero-Navarro[b*], Akira Miura[b] and Kiyoharu Tadanaga[b]

[a.] Graduate School of Chemical Sciences and Engineering, Hokkaido University, Sapporo 060-8628, Japan

[b.] Division of Applied Chemistry, Faculty of Engineering, Hokkaido University, Sapporo 060-8628, Japan

Corresponding Author

*E-mail address: rosero@eng.hokudai.ac.jp

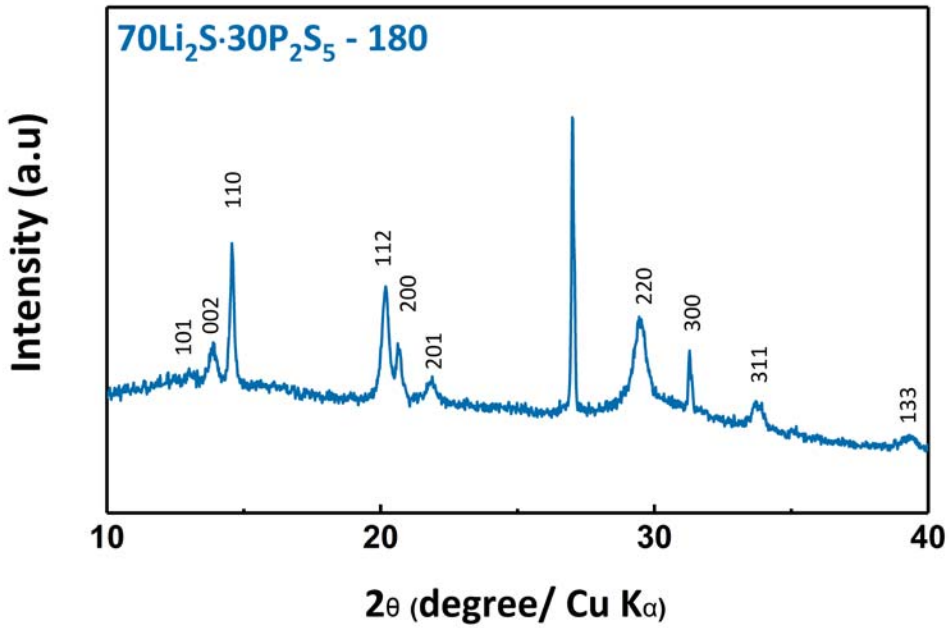

Figure S1. Indexed XRD pattern of the $70Li_2S{\cdot}30P_2S_5$-180 sulfide solid electrolyte.

Table S1. Cell parameters of the $70Li_2S{\cdot}30P_2S_5$-180 sulfide solid electrolyte

a (Å)	8.5930
b (Å)	8.5930
c (Å)	12.7620
α (°)	90
β (°)	90
ɤ (°)	90
Volume ($Å^3$)	942.342
Space group	P4/m(83)

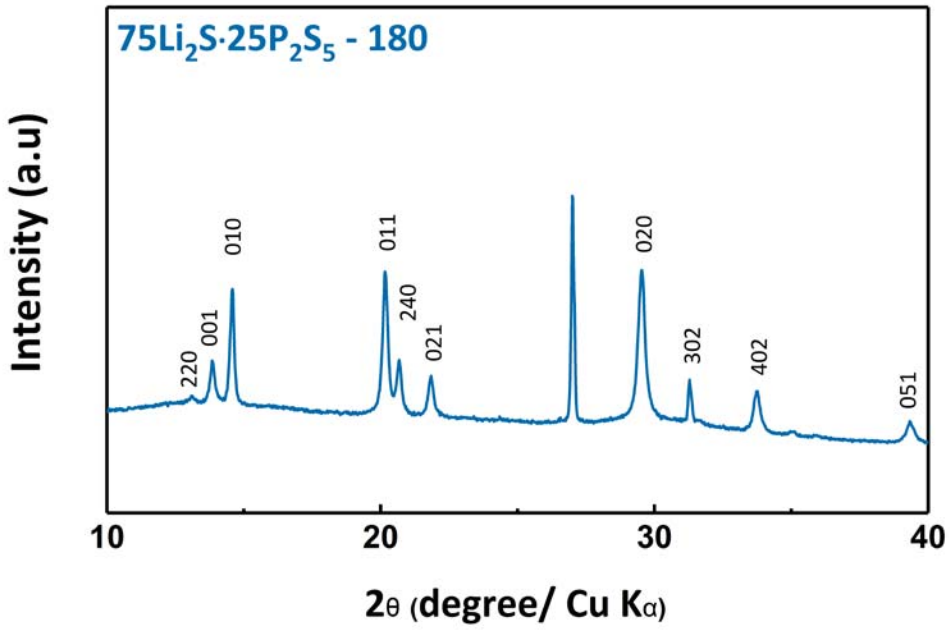

Figure S2. Indexed XRD pattern of the $75Li_2S{\cdot}25P_2S_5$-180 sulfide solid electrolyte.

Table S2. Cell parameters of the $75Li_2S{\cdot}25P_2S_5$-180 sulfide solid electrolyte

a (Å)	19.2157
b (Å)	19.2157
c (Å)	6.3772
α (°)	90
β (°)	90
ɤ (°)	90
Volume ($Å^3$)	2354.737
Space group	P4/m(83)